# Human Arm Stability in Relation to Damping-Defined Mechanical Environments in Physical Interaction with a Robotic Arm

Fatemeh Zahedi and Hyunglae Lee*, *Member, IEEE*

***Abstract*—This paper presents an experimental study that investigated how humans interact with viscous, damping-defined mechanical environments and quantified the lower bounds of robotic damping that they can stably interact with. Human subjects performed posture maintenance tasks for different arm postures while holding a robotic arm manipulator simulating unstable (negative) damping-defined environments and applying rapid perturbations to disturb the arm posture and challenge arm stability. The results of this study demonstrated that the lower bound of robotic damping for stable physical human-robot interaction was more than twice as low in the anterior-posterior (AP) direction than the medial-lateral (ML) direction, with lower limits of -50.3 Ns/m and -21.6 Ns/m in the AP and ML directions, respectively. The results further showed that the human arm is less capable of adjusting to the unstable environments when it is close to the body and laterally displaced for the AP and ML directions, respectively. Secondary analysis on the kinematic response in the phase space also demonstrated that arm stability in the unstable environments can be more easily achieved in the AP than ML direction. The outcomes of this study can be used to design less conservative robotic impedance or admittance controllers that utilize a wider range of robotic damping up to a certain extent of negative damping but do not compromise coupled stability of the human-robot system, which could improve the overall performance in physical human-robot interaction by achieving more agile operations and reducing user effort.**

## I. Introduction

Collaboration and interaction between humans and robots can create many advantages over humans or robots alone. The benefits of such collaboration underscore the importance of physical human-robot interaction (pHRI) in many applications such as exercise therapy in robotic rehabilitation and robotic assistance and augmentation in industrial settings and military applications [1, 2]. Among different robotic platforms, robotic arm manipulators have gained popularity and attracted attention in many pHRI applications [3-6].

When controlling robots that physically interact with humans, it is critical to implement a control system that provides safe and stable interaction between the robot and human without unnecessarily limiting their performance. Among the controllers that have attempted to address safety and stability, impedance or admittance controllers that regulate mechanical impedance, i.e., dynamic behavior at the interaction port often described by stiffness, damping, and inertia, have been used widely and effectively [7-9].

In the past decades, many studies have investigated how human arm impedance is regulated. Most of these studies have focused on quantifying endpoint stiffness, a static component of the arm impedance, and the studies showed how it is modulated and adapted during static posture and dynamic movement tasks under different environmental conditions [10-12].

While this knowledge about human arm stiffness can be utilized in improving the performance of the robotic impedance controllers, arm damping, which is another important component of the arm impedance, can also contribute to the improvement of controller performance since it describes the regulation of the stability of a coupled human-robot system [13, 14]. However, compared to the characterization of arm stiffness, finding a proper identification method to characterize arm damping is challenging since quantification results of this component is highly sensitive to different identification methods [10].

Due to the limited prior research on human arm damping quantification, many current robotic impedance controllers use considerably high positive damping. This conservative control approach shows highly dissipative behaviors to the human user and guarantees the stability during pHRI, but deteriorates the performance in terms of agility and user-effort [15-17]. If it is known how human arm damping is modulated during pHRI, a lower bound of robotic damping of the impedance or admittance controllers could be determined to improve the overall performance without compromising the stability of the coupled human-robot system.

In order to overcome the limitation of directly quantifying the human arm damping and determining the robotic damping accordingly, we proposed an alternative method of quantifying the lower bound of robotic damping that humans can stably interact with by analyzing the kinematic responses of the human arm during interaction with a robotic arm simulating viscous, damping-defined environment. With this method, we could extend the range of robotic damping in pHRI without directly quantifying human arm damping.

Our initial effort to quantify the lower bound of robotic damping for stable pHRI was made for a single arm posture and has been previously presented in [18]. In this previous study, human subjects performed posture maintenance tasks

Research supported by National Science Foundation Award #1846885 and #1925110.

Hyunglae Lee is with the School for Engineering of Matter, Transport, and Energy, Arizona State University, Tempe, AZ 85287, USA (e-mail: hyunglae.lee@asu.edu; 480-727-7463; fax: 480-727-9321).

Fatemeh Zahedi is with the School for Engineering of Matter, Transport, and Energy, Arizona State University, Tempe, AZ 85287, USA (e-mail: fzahedi1@asu.edu).

*: corresponding author

within a predefined range of negative damping-defined environments while their arm was perturbed to challenge postural stability. However, the quantification was made only at a single arm posture due to lengthy experiments requiring brute force exploration to find the lower bound. While this preliminary study provided useful baseline information, the information gained cannot be directly applied to general arm movement tasks covering a wide range of motion.

Our goal in this paper is to quantify the lower bound of robotic damping that humans can stably interact with for various arm postures covering most of the reachable space during natural arm motions. To determine the lower bound in each arm posture without lengthy experiments that might cause subject fatigue, experiments were optimized using the bisection algorithm and the baseline information about the lower bound of robotic damping from the previous study. Thus, we could successfully overcome the time limitation of the previous study and determine the lower bound of robotic damping for stable pHRI for various arm postures.

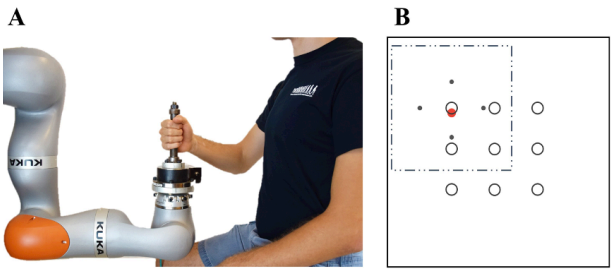


**Fig. 1.** Experimental setup. **A**: Side view of the robotic arm coupled to a human subject in the neutral position. **B**: Visual feedback display. Black hollow circles showed 9 different targets for different arm postures. The red solid circle presented the current hand position. Small gray circles were at ±5 cm from the current target position appeared at the beginning of each trial either in the AP direction or ML direction to help subjects explore the simulated mechanical environment. Dotted lines denote the boundaries of the virtual walls around the target position. The solid lines showed the boundaries of the virtual walls around the whole plane of movement.

## II. Methods

### A. Experimental Setup

A 7 degree-of-freedom (DOF) robotic arm (LBR iiwa R820, KUKA, Germany) with a 6-axis load cell (Delta IP60, ATI Industrial Automation, NC) were used to evaluate the human arm stability during interaction with unstable damping-defined environments in different arm postures. Both kinematic and force data were recorded at 1 kHz and low-pass filtered using a bi-directional 4th order Butterworth filter with a cutoff frequency of 20 Hz to remove the high-frequency noise.

Two distinct controllers have been implemented: 1) an admittance controller to simulate unstable (negative) damping-defined environments and 2) a position controller to apply fast perturbation to disturb the arm posture and challenge arm stability in either the anterior-posterior (AP) or medial-lateral (ML) direction. The robot alternated between these two controllers in a sample time of 1 ms. This small delay provided a transient position perturbation to the arm during interaction with the simulated mechanical environments.

Subjects were seated with their trunk securely strapped to a rigid chair and instructed to hold a handle connected to the robot end-effector (Fig. 1A). Arm stability was evaluated around the neutral arm posture, defined as follows: shoulder in ~70° of abduction, ~45° of horizontal flexion, and the elbow in ~90° of flexion.

A visual feedback display (at a distance of ~1 m from the subject) helped subjects to complete posture maintenance tasks by showing current and target hand positions (Fig. 1B). Nine evenly distributed points around the neutral posture (±6 cm in the AP and ML directions) were tested. These nine points were chosen to cover the whole accessible workspace of the arm in the horizontal plane.

A high stiffness of $10^6$ N/m was simulated in the vertical plane to constrain vertical arm movement and only allow for horizontal plane movement. In the horizontal plane, zero stiffness and a constant inertia of 10 kg were simulated, and only robotic damping was varied to manipulate the level of environmental stability. The ramp position perturbation had an amplitude of 5 cm with an average speed of 20 cm/s. Our previous study has performed a sensitivity analysis with varying inertias and perturbation profiles and has demonstrated their minimal impact on arm postural stability [18].

Arm stability in both the AP and ML directions was tested in each of the 9 arm postures. During trials in the AP direction, the robotic damping in the ML direction was constant at 30 Ns/m and the damping in the AP direction was varied. Similarly, during trials in the ML direction, the robotic damping in the AP direction was constant at 30 Ns/m and in the ML direction was varied. The damping in the AP direction was varied from the initial value of -30 Ns/m, and iteratively subtracted by 10 Ns/m until the human arm could no longer stably interact with the simulated damping. If the arm failed to stabilize at the initial value, the damping was iteratively added by 10 Ns/m until stable interaction was achieved. From this point, the damping was changed based on the bisection method until the difference of the damping values for stable interaction and unstable interaction was less than 5 Ns/m. The damping value for the final successful trial was regarded as the lower-bound of robotic damping that the human arm could stably interact with. The same algorithm was implemented for the ML direction, except that the initial damping was -10 Ns/m and the initial changing interval until the first failed trial was 5 Ns/m. These values were chosen based on preliminary experiments and previous findings in [18].

As a safety feature, two virtual walls were implemented. One was a virtual wall of 40 x 40 $cm^2$ around the whole 9 arm postures. High stiffness was implemented out of this virtual wall to prevent any displacement outside of these boundaries. The other was a virtual wall of 24 x 24 $cm^2$ around each target position (Fig. 1B). If displacement reached this virtual wall, the simulated damping switched to 30 Ns/m to stabilize the arm and prevent any potential injuries.

Ten young, healthy subjects (age: 20–33, height: 162–186 cm, weight: 47–86 kg, sex: 7 males and 3 females) participated in this study, which was approved by the Institutional Review Board of Arizona State University (STUDY 00010123). Subjects provided informed, written consent prior to participation. All experimental procedures were performed in accordance with the relevant guidelines and regulations. No subject was informed regarding the purpose of this study.

### *B. Experimental Protocol*

An experiment was designed in which subjects performed posture maintenance tasks in 9 different arm postures in both the AP and ML directions. First, the target position and the direction of movement were randomly selected among the 9 arm postures. Subjects were instructed to explore the selected damping-defined mechanical environment by reaching the small gray circles on the visual feedback display (Fig. 1B) that were 5 cm apart from the chosen target position, and then to return to the target position (±5 mm). After the target position was maintained for a randomized time interval of 0.5–1.5 s, the position perturbation displaced the arm to disturb the current arm posture and challenge arm stability. Subject were instructed to move their arm back to the target position as efficiently as possible following the perturbation.

The damping-defined mechanical environment that subjects need to explore changed according to the setup mentioned in the previous subsection. The damping value defining the mechanical environment started from the initial condition until it converged to the lower bound of damping. After the lower bound of damping was found for the selected target position, the next target position was chosen randomly, and the process was repeated. The process of the experiment is presented in Algorithm 1, which explains with more details about how the previously described method works to find the lower bound of robotic damping in different arm postures. B is denoted as the robotic damping.

A total of 18 experimental conditions (9 target positions x 2 directions) were tested. These experimental conditions were divided into 9 blocks in order to avoid subject fatigue. On average, each of these conditions took 7 trials to converge to the lower bound, resulting in a total of 126 trials. Two additional training blocks were provided before the main experiment to help subjects familiarize themselves with the experimental setup and protocol. The entire experiment, including these two training blocks and rest periods, took under 30 mins.

### *C. Data Analysis*

For each trial, the negative robotic damping value defining the unstable mechanical environment was chosen based on the success or failure of the previous trial. A trial was considered successful if subjects maintained the hand position inside the target position (±5 mm) for 500 ms continuously after the perturbation within 3 s. If subjects failed to meet this criterion or if the hand position passed the boundaries of the virtual wall around the current target position (either in the exploration phase or after perturbation), this trial was considered failed.

**Algorithm 1** Finding the lower bound of robotic damping that humans can stably interact with

**while** isempty $\boldsymbol{B_{lowerbound}}$ of any target position and perturbation direction **do**
  Select the target position randomly
  Select the direction of movement randomly
  Initialization interval_change & initial_condition based on direction
  B ← initial_condition
  **while** success_bound isempty || failed_bound isempty **do**
  Test trial with B
  **if** trial succeed **then**
    success_bound ← B
    B ← B – interval_change
    **else**
      failed_bound ← B
      B ← B + interval_change
  **end while**
  **while** |success_bound – failed_bound| > 5 **do**
    B ← $\boldsymbol{(success\_bound + failed\_bound)/2}$
    Test trial with B
    **if** trial succeed **then**
      success_bound ← B
    **else**
      failed_bound ← B
  **end while**
  $\boldsymbol{B_{lowerbound}}$ ← success_bound
  **return** $\boldsymbol{B_{lowerbound}}$ to selected target position and direction
**end while**

Nine different arm postures in both the AP and ML directions were tested for each subject to find the lower bound of robotic damping that the subject can successfully interact with. For each of the 18 experimental conditions, group results were reported by calculating the average of the lower bound damping of all 10 subjects, which show the differences of the lower bound of robotic damping with respect to the direction of movement and distance of the arm to the body.

Besides the analysis in the time domain, kinematic stability was also investigated in a phase space consisting of phase variables of position and velocity. In particular, for each of the 9 arm postures, successful trials at the lower bound of robotic damping were analyzed to identify any differences between the AP and ML directions regarding the margin of stability.

In the phase space analysis, the rate of reduction in the kinematic error after perturbation was calculated. Two-dimensional (2D) phase variables $X = [p \quad v]$ were defined where $p$ and $v$ were position and velocity, respectively. To lessen the burden in computation without losing the details, the raw data of position and velocity were down sampled by averaging data points within a 50 ms window. Using the down-sampled data, phase arrays, $\vec{X}(k)$ and $\vec{X}(k+1)$, were further defined as:

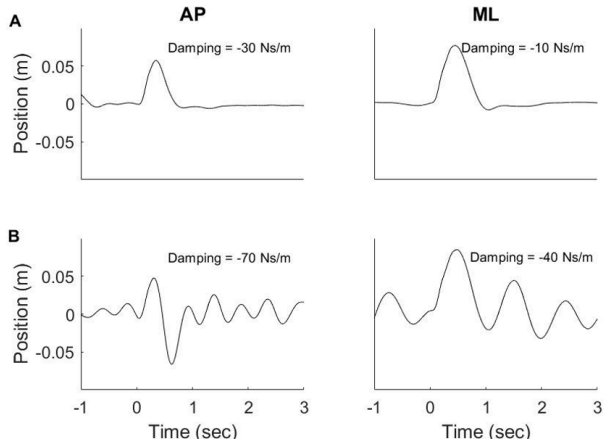


**Fig. 2.** Kinematic responses of the arm endpoint of a representative subject for the AP and ML directions. Endpoint positions are presented for the time interval of [-1, 3] s, where 0 s is the onset of the perturbation. **A**: successful trials, **B**: failed trials. (Left): kinematic responses in the AP direction, (right): kinematic responses in the ML direction. The corresponding robotic damping value was included in each plot.

$$\vec{X}(k) = \begin{bmatrix} p(k_1) & v(k_1) \\ p(k_2) & v(k_2) \\ \vdots & \vdots \\ p(k_{n-1}) & v(k_{n-1}) \end{bmatrix}, \quad \vec{X}(k+1) = \begin{bmatrix} p(k_2) & v(k_2) \\ p(k_3) & v(k_3) \\ \vdots & \vdots \\ p(k_n) & v(k_n) \end{bmatrix} \tag{1}$$

where $k_1$ and $k_n$ was the moment corresponding to the end of the ramp position perturbation and the first moment that subjects maintained the hand position inside the target for 500 ms continuously following the perturbation, respectively. The relationship between $\vec{X}(k)$ and $\vec{X}(k+1)$, potentially nonlinear, was linearized with respect to the target position and represented by a 2D Jacobian matrix $J_f$:

$$\vec{X}(k+1) = J_f \vec{X}(k). \tag{2}$$

The maximum eigenvalue of $J_f$ was calculated to quantify the rate of contraction of the phase variables in the phase space. The system is stable as long as the eigenvalue is less than 1. In addition, the higher the maximum eigenvalue, the less the stability margin.

Statistical analysis was performed to investigate the direction dependence (AP vs. ML) of arm stability for all of the 9 arm postures. A paired t-test was performed separately for the lower bound of robotic damping from the time domain analysis and the maximum eigenvalue from the phase space analysis.

## III. Results

All subjects could stably interact with unstable viscous (negative damping-defined) environments to a certain extent, but the time and effort needed to stabilize the arm increased as the level of environmental stability decreased,

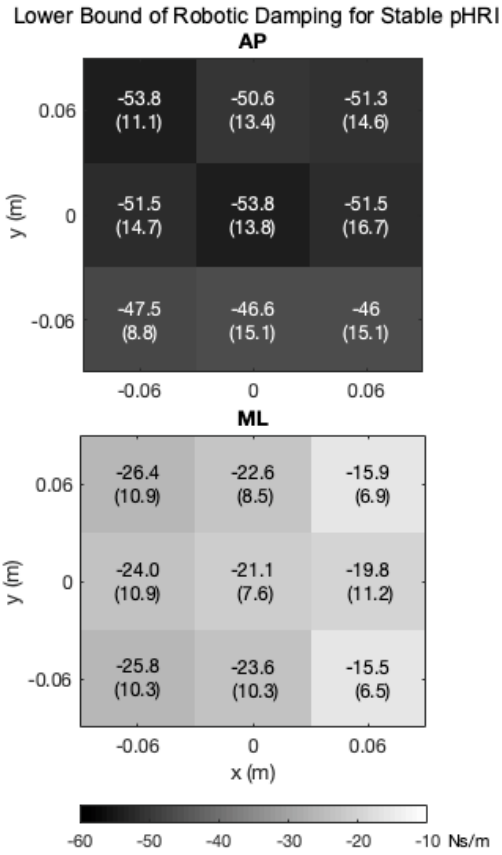


**Fig. 3.** Lower-bound of robotic damping that the human arm can stably interact with for each of the 9 testing postures for AP (top) and ML (bottom) directions. The mean and standard deviation (in parentheses) of 10 subjects are presented.

i.e., robotic damping decreased. The lower bound of robotic damping that subjects could stably interact with was determined based on successful and failed trials, which varied for different arm postures and perturbation directions.

Kinematic responses of the arm endpoint of a representative subject for the AP and ML direction trials are presented in Fig. 2. The difference between successful and failed trials is clear from this figure. In the successful trials, in both directions, subjects could stabilize the arm with minimal oscillations, while in the failed trials they could not regain posture stability.

The bisection algorithm with the baseline information about the lower bound from the previous study [18] greatly decreased the number of trials and time required for finding the lower bound of robotic damping for stable pHRI. The number of trials to find the lower bound for each posture and each direction was less than 8 trials on average across all 10 subjects. The previous study, by comparison, required 240 trials to find the lower bound for a single posture, the neutral position, in both the AP and ML directions [18], which is about 15 times more than that in this study.

Group analysis on 10 subjects demonstrated that, on average across all 9 different postures, the lower bound of robotic damping that the human arm can stably interact with was significantly lower in the AP direction than ML

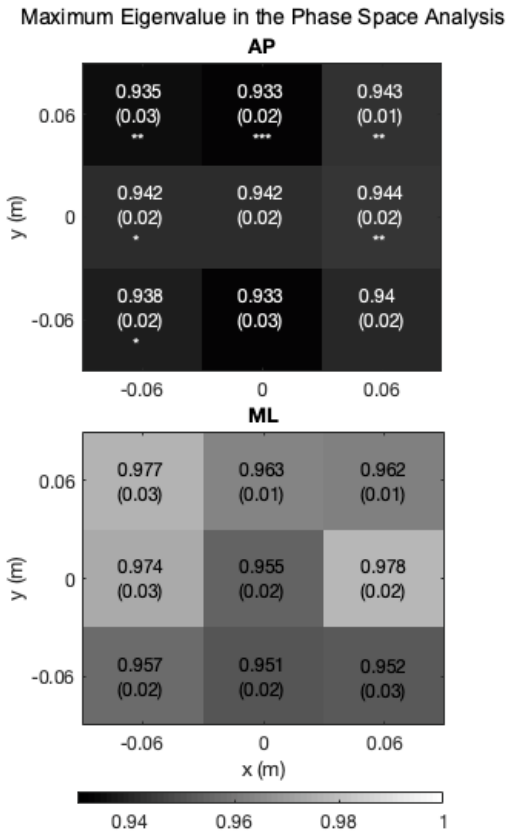


**Fig. 4.** Maximum eigenvalues from the phase space contraction analysis. The values were calculated in the lower bound condition for each of the 9 testing postures for the AP (Top) and ML (Bottom) directions. The corresponding statistical analysis results between the AP and ML directions for each posture were denoted with asterisks in the top plot (*: $p < 0.05$, **: $p < 0.01$, ***: $p < 0.001$). The mean and standard deviation (in parentheses) of 10 subjects are presented.

direction: -50.3 (2.9) Ns/m and -21.6 (4.0) Ns/m for the AP and ML directions, respectively. Results for each of the 9 testing postures are shown in Fig. 3. The minimum lower bound in the AP direction was -53.8 Ns/m for the arm posture furthest from the body. The minimum value for the ML direction was -26.4 Ns/m for the same arm posture as in the AP direction.

For any of the 9 arm postures, the statistical analysis with the paired t-test confirmed that the lower bound was significantly lower in the AP than ML direction ($p < 0.0005$). A higher arm stability in the AP than ML direction is consistent with previous findings that human arm impedance is significantly higher in the AP than ML direction [11, 19].

Group results also demonstrated that the human arm is less capable of adjusting to unstable damping-defined environments when it is closer to the body in the AP direction, and when it is laterally displaced in the ML direction.

According to the phase space analysis, the maximum eigenvalue of the Jacobian matrix ($J_f$) was always less than 1 for any successful trial with the identified lower bound of robotic damping, implying stable pHRI.

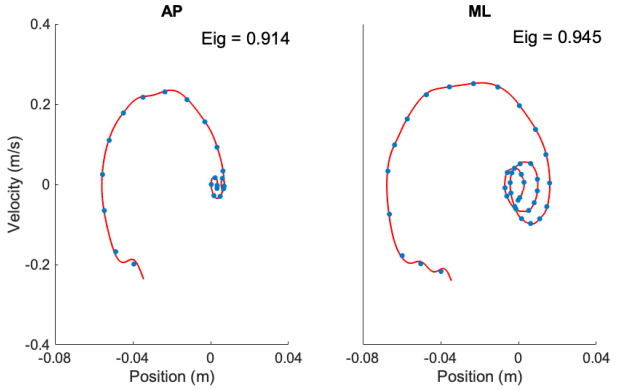


**Fig. 5.** Representative results of state trajectories (endpoint velocity vs. position) in the phase space for the AP and ML directions in the same posture in the lower bound condition. Red traces represent raw data sampled at 1 kHz, and blue dot points represent down-sampled data points. The corresponding maximum eigenvalue was included in each plot.

Group results of the phase space analysis also confirmed that the stability margin is greater in the AP than ML direction, evidenced by the lower maximum eigenvalue of $J_f$ in the AP direction (Fig. 4). In all 9 arm postures, the average eigenvalue in the AP direction was lower than that in the ML direction, and 6 postures showed statistical difference. This result demonstrates that arm stability at the lower bound of robotic damping conditions for stable pHRI can be more easily achieved in the AP than ML direction. In other words, subjects had more difficulty in reducing the kinematic error induced by the position perturbation during interaction with an unstable environment in the ML than AP direction. The sample results of a representative subject showed higher overshoots, oscillations, and slower convergence to the target position in the ML than AP direction for the related lower bound condition (Fig. 5). These results are consistent with the results of the time domain analysis.

## IV. Discussion

Compared with human arm stiffness, arm damping has been relatively understudied. This is mainly because damping quantification is more sensitive to different identification methods than other impedance parameters. A lack of knowledge about human arm damping has prompted excessively conservative robotic impedance controllers with significant positive damping, which sacrifices the overall performance in pHRI at the expense of stability. With the knowledge about human arm damping modulation, impedance controllers could utilize a wider range of robotic damping values to the improve the overall performance, for example, increasing agility of the coupled human-robot system and decreasing user effort.

In order to overcome the limitation of directly quantifying the human arm damping and determining a proper range of robotic damping that could improve the overall performance of the coupled human-robot system, we quantified the lower bound of robotic damping that humans

can stably interact with, which will be used to directly determine the range of robotic damping for the performance improvement. To this end, we analyzed the kinematic responses of the human arm, in both the time domain and phase space, during interaction with a robotic arm simulating viscous, damping-defined environment. In order to cover most of the reachable space during natural arm motions, the study was performed at 9 different arm postures around the neutral arm posture. With the bisection algorithm and the baseline information about the lower bound of robotic damping from the previous study, we could substantially reduce the time required for the quantification by a factor of 15 compared to the previous brute force approach in [18].

The results of this study demonstrated that the lower bound of robotic damping that the human arm can stably interact with is more than twice as low for the AP direction than for the ML direction. The statistical analysis confirmed that the difference of lower bound in AP and ML direction in all 9 arm postures is significant. The results also showed that the arm is less capable of adjusting to unstable damping-defined environments when it is closer to the body and when it is laterally displaced for the AP and ML directions, respectively. Finally, the phase space analysis further supported that arm stability at the lower bound of robotic damping conditions is more easily achieved in the AP than ML direction. In other words, the stability margin was greater in the AP than ML direction. These results are consistent with the previous findings that human arm impedance is significantly higher in the AP than ML direction and exhibits posture-dependent characteristics.

Outcomes of this study, i.e., lower bounds of robotic damping for stable pHRI in different arm postures and in both the AP and ML directions, will guide us to carefully design robotic impedance controllers that are applicable to complicated tasks requiring a wide range of motion, as is common in many real-world tasks. The impedance or admittance controllers with this bound information will avoid imposing unnecessarily high damping but utilize a wider range of robotic damping from negative to positive values to improve the trade-off between stability and performance (e.g., agility and user effort) without compromising the coupled stability of the human-robot system [20-22].

## REFERENCES


[1] Krebs, H.a. and B. Volpe, Rehabilitation robotics, in Handbook of clinical neurology. 2013, Elsevier. p. 283-294.

[2] Heyer, C. “Human-robot interaction and future industrial robotics applications.” In IEEE/RSJ International Conference on Intelligent Robots and Systems. 2010.

[3] S. Haddadin, M. Suppa, S. Fuchs, T. Bodenmuller, A. Albu-Schaffer, and G. Hirzinger, Towards the robotic co-worker (Robotics Research). Springer, 2011, pp. 261-282.

[4] P. Tsarouchi, S. Makris, and G. Chryssolouris, "Human–robot interaction review and challenges on task planning and programming," International Journal of Computer Integrated Manufacturing, vol. 29, no. 8, pp. 916-931, 2016.

[5] A. Albu-Schaffer, S. Haddadin, C. Ott, A. Stemmer, T. Wimbock, and G. Hirzinger, "The DLR lightweight robot: design and control concepts for robots in human environments," Industrial Robot-an International Journal, vol. 34, no. 5, pp. 376-385, 2007.

[6] C. Ott, O. Eiberger, W. Friedl, B. Bauml, U. Hillenbrand, C. Borst, ¨ A. Albu-Schaffer, B. Brunner, H. Hirschmuller, S. Kielhofer, R. Koni- ¨ etschke, M. Suppa, T. Wimbock, F. Zacharias, and G. Hirzinger, “A humanoid two-arm system for dexterous manipulation,” in 6th IEEE-RAS International Conference on Humanoid Robots, Genova, pp. 276–283, December 2006.

[7] N. Hogan, "Impedance Control - an Approach to Manipulation .1. Theory," Journal of Dynamic Systems Measurement and Control-Transactions of the Asme, vol. 107, no. 1, pp. 1-7, 1985.

[8] N. Hogan and S. P. Buerger, "Impedance and interaction control," Robotics and Automation Handbook, New York, CRC Press, 2005.

[9] T. Tsumugiwa, R. Yokogawa, and K. Hara, "Variable impedance control based on estimation of human arm stiffness for human-robot cooperative calligraphic task," in IEEE International Conference on Robotics and Automation (ICRA), Washington D.C., USA, pp. 644-650, 2002.

[10] E. Burdet, R. Osu, D. W. Franklin, T. Yoshioka, T. E. Milner, and M. Kawato, "A method for measuring endpoint stiffness during multi-joint arm movements," J Biomech, vol. 33, no. 12, pp. 1705-9, Dec 2000.

[11] E.J. Perreault, R.F. Kirsch, and P.E. Crago, “Effects of Voluntary Force Generation on the Elastic Components of Endpoint Stiffness,” Experimental Brain Research, vol. 141, pp. 312-323, 2001.

[12] M. A. Krutky, R. D. Trumbower, and E. J. Perreault, “Influence of environmental stability on the regulation of end-point impedance during the maintenance of arm posture,” J. Neurophysiol., vol. 109, no. 4, pp. 1045–1054, 2013.

[13] H. Cho and J. Park, “Impedance Control with Variable Damping for Bilateral Teleoperation under Time Delay,” JSME Int’l J. Series C, vol. 48, no. 4, pp. 695-703, 2005.

[14] D. Surdilovic, “Contact stability issues in position based impedance control: Theory and experiments,” in Proc. IEEE Int. Conf. Robotics and Automation, pp. 1675–1680, 1996.

[15] C. Ott, A. Albu-Schaffer, A. Kugi, and G. Hirzinger, “On the passivity-based impedance control of flexible joint robots,” IEEE Transactions on Robotics, vol. 24, no. 2, pp. 416–429, 2008.

[16] G. Raiola, C. A. Cardenas, T. S. Tadele, T. De Vries, and S. Stramigioli,“Development of a safety-and energy-aware impedance controller for collaborative robots,” IEEE Robotics and automation letters, vol. 3, no. 2, pp. 1237–1244, 2018.

[17] H. Lee and N. Hogan, "Essential considerations for design and control of human-interactive robots," in In Proc. 2016 IEEE International Conference on Robotics and Automation (ICRA), Stockholm, pp. 3069-3074, 2016.

[18] F. Zahedi, T. Bitz, C. Phillips, and H. Lee, "Regulation of 2D Arm Stability against Unstable, Damping-Defined Environments in Physical Human-Robot Interaction," International Conference on Intelligent Robots and Systems (IROS), 2020.

[19] H. Gomi and R. Osu, "Task-dependent viscoelasticity of human multijoint arm and its spatial characteristics for interaction with environments," *J Neurosci,* vol. 18, no. 21, pp. 8965-78, 1998.

[20] T. Bitz, F. Zahedi, and H. Lee, "Variable Damping Control of a Robotic Arm to Improve Trade-off between Agility and Stability and Reduce User Effort," in IEEE International Conference on Robotics and Automation (ICRA), France, 2020.

[21] J. Arnold, H. Hanzlick, and H. Lee, "Variable Damping Control of the Robotic Ankle Joint to Improve Trade-off between Performance and Stability," in IEEE International Conference on Robotics and Automation (ICRA), Montreal, Canada, pp. 1699-1704, 2019.

[22] J. Arnold and H. Lee, " Variable Impedance Control for pHRI: Impact on Stability, Agility, and Human Effort in Controlling a Wearable Ankle Robot," IEEE Robotics and Automation Letters (RA-L), vol. 6, no. 2, pp. 2429-2436, 2021.